VOLCANICA Article in Press

This is an uncorrected proof, meaning that this manuscript has not been copyedited or formatted according to Volcanica's styles and standards. In turn, this means that article content, including text, may still change prior to final publication. Although articles in press do not have all bibliographic details available yet, they can be cited using the year of online publication and the DOI, as follows: author(s)(year), article title, Volcanica, DOI.

Márquez-Ramírez, V. H., Capra, L., Avila, P. C., Alonso Rivera, P. and Castelán, G. (2026) "Seismic characterization of rainfall-triggered lahars at Popocatépetl volcano: first results from real-time monitoring", Volcanica, 9(2). doi: 10.30909/vol/vkhf1063.

article in press

Seismic characterization of rainfall-triggered lahars at Popocatépetl volcano: first results from real-time monitoring

V.H. Márquez-Ramírez[1*], L. Capra[1], P.C. Ávila[2], P. Alonso Rivera[2], G. Castelán-Pescina[2]

1. Instituto de Geociencias, Campus UNAM-Juriquilla, Querétaro, México.
2. Centro Nacional de Prevención de Desastres (CENAPRED), Ciudad de México, México.

*marvh@geociencias.unam.mx

ORCiD **(VHMR):** 0000-0003-1494-2229
ORCiD **(LC):** 0000-0003-3973-7264

article in press

Abstract

Popocatépetl is one of the most active volcanoes in Mexico; the seismic characterization of its rainfall-triggered lahars has not yet been systematically documented. We present the first seismic analysis of nine lahars recorded during the 2025 rainy season at a monitoring station on the NW flank, 5.4 km from the crater along the Huiloac–Tenenpanco drainage. Time-frequency analysis of the vertical component shows amplitudes from 10^{-2} to 10^{-1} mm/s for most events, peaking at 1.19 mm/s on 21 August 2025. Three distinct signal types were identified from Power Spectral Density (PSD) distributions with dominant content between 5 and 30 Hz. A positive correlation between amplitude and PSD peak frequency in the 5–22 Hz range allows for the differentiation of hyperconcentrated flows and fluvial events, consistent with Volcán de Colima. Rainfall thresholds of >9 mm accumulated and >25 mm/hr peak intensity trigger lahars. At Popocatépetl volcano, a seismic detection threshold of 1 mm/s is proposed to support the development of an operational early warning system.

Non-technical summary

Popocatépetl is one of the most active volcanoes in the world and threatens more than 20 million people in central Mexico, including the major population centers of Mexico City and Puebla. Among its hazards, lahars can travel kilometers down its slopes and reach nearby towns. Until now, however, there was no continuous record of these flows at this volcano. We installed a station on the volcano's northwest flank that combines ground-vibration sensors, a video camera, and a rain gauge, and we used it to monitor the 2025 rainy season. We detected nine lahars and measured

their strength, the vibration frequencies they produced, and the rainfall that triggered them. By comparing them with similar flows at Volcán de Colima, we identified rainfall amounts and vibration levels that signal a potentially dangerous flow. These thresholds are the first step toward an early warning system that can alert downstream communities in time.

1. Introduction

Lahars are volcanic processes that can threaten areas around volcanoes during both eruptions and periods of dormancy (Thouret et al., 2020). They consist of a fast-moving mixture of water and rock debris eroded from the volcano's slopes (Smith and Lowe, 1991), and their magnitude is heavily influenced by the amount of available water and the amount of unconsolidated material incorporated. Typically, the water source is rainfall, but it can also come from glacier melting (Nevado del Ruiz, Nevado del Huila, Colombia, Huggel et al., 2007) or lake breakouts (Mt Ruapehu, New Zealand; Carrivick et al., 2009; Chichon, Mexico, Macías et al., 2004). Their characterization is mainly based on field study of the associated deposits (e.g. Pierson and Scott, 1985; Lavigne and Thouret., 2002; Barclay et al., 2007) or from real-time monitoring (e.g. Lavigne et al., 2000; Doyle et al., 2011; Bosa et al., 2021; Bosa et al., 2024; Bejar et al., 2026). In the first case, characteristics of the event can be inferred from the textural features and geometry of the deposits (Scott et al., 1995), and, using real-time monitoring, some flow features can be directly measured, such as flow depth and velocity, and a semi-quantitative estimate of sediment content (Doyle et al., 2011; Coviello et al., 2018). These data are critical for hazard map construction and setting up an early warning system.

Popocatépetl is the most active volcano in Mexico (Figure 1a), and its recent unrest began in 1994. The volcano threatens more than 20 million people, including Mexico City and the Puebla basin, where extensive deposits of pyroclastic density currents (PDCs) and pumice falls were emplaced during earlier eruptive activity, especially after its partial collapse at 23.5 ka BP (Siebe et al., 2017). Among the most catastrophic eruptions, at least five Plinian phases have been documented (Siebe et al., 1996; Sosa-Ceballos et al., 2012; Siebe et al., 2024), with the emplacement of PDC and pumice fall deposits that, when remobilized, caused massive syn- and

article in press

post- eruptive lahars (Siebe et al., 1999). Since 1994, minor activity has resumed, marked by small Vulcanian eruptions involving the disintegration of small domes and the formation of eruptive columns reaching 2-3 km in height that disperse ash across the region. The December 2000-January 2001 eruptive phase was the largest recorded recently, producing an 8 km-high eruptive column and PDCs that traveled up to 4 km toward the N- NE (Macías et al., 2020). At that time, an ice cap was still present, and a lahar originated five hours after the PDC was emplaced, reaching a small town 15 km from the crater (Capra et al., 2004). One of the main active ravines for lahar formation runs along the Huiloac-Tenenpanco drainage on the NW flank of the volcano, which drained water from the glacier until 2003. This study presents the first seismic analysis of lahars at Popocatépetl volcano, obtained from a monitoring site located on the NW flank, at 5.4 km from the crater. Data from lahars recorded during the 2025 rainy season are presented and analyzed to examine their seismic features, including amplitude and frequency as indicators of flow magnitude and sediment content, along with rainfall patterns that triggered the recorded events. The data in this paper represent the first effort to establish an early-detection system for lahars at Popocatépetl, which could help reduce risks associated with one of the most common phenomena linked directly or indirectly to the volcano's eruptive activity.

2. Historical and recent lahars at Popocatépetl volcano.

Lahars have been commonly recorded in the eruptive history of Popocatépetl volcano. The largest events were associated with major Plinian eruptions and occurred not only on the volcano's slopes but also in ravines draining from Iztaccihuatl volcano, which were extensively covered by pumice and ashfall during these eruptions. These lahars inundated the Puebla and Mexico basins, affecting human settlements during the pre- and post-classic eras (Siebe et al., 1999). During the Late Holocene, the interaction between eruptive activity and the presence of an ice cap promoted the formation of lahars along the Huiloac ravine (Figure 1). The best example is the San Nicolas lahar, which occurred at 1100-1300 yr BP and reached distances of up to 57 km from source (González, 2000). More recently, at

article in press

least two additional glacier-related events occurred: one in 1998 and another in 2001, both directly related to the interaction between the ice cap and the ongoing activity. In particular, the 2001 lahar originated five hours after the emplacement of a pumice flow deposit that eroded the glacier on the proximal reach of the Huiloac watershed, reaching the town of Santiago Xalitzintla 15 km from the crater (Capra et al., 2004; Muñoz-Salinas et al., 2009). In terms of volume, these events were similar, on the order of 10^5 m^3 (Table 1). Lahars were also generated from shallow landslides (Hungr et al., 2014) in response to extreme hydrometeorological events, as observed in 1995 and 2010 in the Nexpayantla ravine on the western flank of the volcano (Zaragoza et al., 2020), or during major earthquakes, such as the 7.1 Mw event on September 19, 2017, with an epicenter just 70 km from the volcano. The strong acceleration triggered several mass-wasting processes in the area, including hundreds of soil slips on the volcano's western flank, where a lahar of 10^6 m^3 in volume infilled the Huitzilac ravine and reached the main interstate road near the town of Atlautla (Coviello et al., 2021). None of the events mentioned above resulted in fatalities.

3. Methods

3.1 Characteristics of the monitoring site

The monitoring site (HMS), located at the outlet of the watershed that drains from the northern flank of the cone to the Huiloac ravine, is 5.4 km from the crater and 8 meters from the channel (Figures 1b and 2a). It includes a Raspberry Shake 4D (RS-4D;v.6), a low-cost instrument with a single vertical-component 4.5 Hz geophone with the corner frequency electronically extended to 0.5 Hz and a three-component Micro-Electro-Mechanical Systems (MEMS) accelerometer. All the signals were digitized at 24 bits and sampled at 100 samples per second (Anthony et al., 2019). Only the vertical geophone data were analyzed here. Additionally, the monitoring site includes a Mobotix camera capturing images at 704x480 px in resolution, and a tipping-bucket rain gauge recording rain accumulation at 5 min intervals (0.2 mm resolution, HOBO®). All data are transmitted in real time to Centro Nacional de

article in press

Prevención de Desastres (CENAPRED) via a repeater on Tlamacas peak (TL, Figure 1b). The monitoring site was installed in 2019, but a continuous transmission system was achieved only in 2024. Finally, the data transmission is interrupted during heavy rainfall events, and images are not stored locally, so they are not always available for detected events.

3.2 Seismic analysis

Time-frequency analysis was performed on all 2025 vertical-component seismic records. Processing began with correction for instrument response, followed by the removal of the mean and linear trend from each signal. Each signal was high-pass filtered with a corner frequency of 1 Hz. This corner frequency was selected for two reasons. First, although the geophone has a natural frequency of 4.5 Hz, with its response electronically extended to 0.5 Hz, filtering below 1 Hz would amplify instrument noise rather than recover ground motion. Second, previous studies indicate that lahar signals fall within a frequency range above 1 Hz (Doyle et al., 2010; Bosa et al., 2024; Bejar et al., 2026; Gheri et al., 2026). This choice, moreover, facilitates a direct comparison with lahars documented at other volcanoes such as Volcán de Colima (Vázquez et al., 2016; Martínez-Valdés et al., 2023; Márquez-Ramírez et al., 2025). The peak absolute ground-motion amplitude was measured in millimeters per second (mm/s). Power spectral densities (PSDs) were computed using Welch's method (Welch, 1967), and spectrograms were computed using the Short Time Fourier Transform (STFT), both employing a 10-second window with a standard 50% overlap to minimize spectral variance. This window length provides a suitable compromise between spectral resolution and quasi-stationarity, which is critical given the strongly non-stationary nature of seismic lahar signals (Tary et al., 2014).

3.3 Hydrological characteristics and Rainfall data

A 5-m DEM of the volcano slope was used for hydrologic analysis. ArcGIS Pro was employed to delineate the main watersheds and their extents. Rainfall data from

article in press

2025 were processed to identify rainfall events (separated by a dry period of > 1 hr). For each event, the total rainfall accumulation (R), duration (D), average intensity (I_A: R/D), and maximum peak intensity (I_5, computed over a window of 5 min) were calculated (Table 2 and Table S1 in supplementary material). Because rainfall can be spatially variable, the data collected at the monitoring station may not align in time with lahar initiation, which occurs in the upper portion of the watershed. Despite this approximation, the rainfall data were analyzed to identify a possible threshold for lahar triggering. Total accumulated rainfall from the Tenenepanco station (TN, Figure 1b, R* in Table 2), provided by CENAPRED, is also included to better observe the spatial rainfall variability.

3.4 Image analysis

Still images captured by the monitoring-site camera were used to qualitatively describe the lahars detected in 2025, including estimated flow depth and morphological changes in the channel before and after each event. The scale was derived from an image taken in October 2025 (Figure 2c). Older images were used as a reference to characterize past events for which seismic records are not available, also providing a better scale for comparison with the lahar detected in 2025.

4. Results

4.1 Seismic characteristics

By analyzing the 2025 daily helicorders, nine events were manually detected (Figure 3 and Table 1). As the volcano is highly active, the seismic records include volcanic-tectonic (VT) events, tremors, and explosions. The main criteria for differentiating a lahar from other volcanic events were the duration and the frequency of the signal. VT events and explosion have very short durations compared to a lahar; tremors can last for several minutes or hours, but their frequency content is below 1 Hz in contrast to a lahar, whose main frequency range is between 10 and 50 Hz (Vázquez et al., 2016; Arámbula-Mendoza et al., 2016; Zobin, 2017).

article in press

All the events display the typical wave shape of a lahar, with an emergent rise in amplitude as the flow reaches the monitoring station, followed by a gradual decrease in the signal (Figure 3a). On average, the amplitude of the detected events ranges from 10^{-2} to 10^{-1} mm/s, except for the event recorded on 21 August 2025 (#233, Table 1), which has a maximum amplitude of 1.19 mm/s. The frequency spans the 1-50 Hz frequency band, but based on the PSD energy, three main signal types can be identified (Figure 3b and 4): a) with a main frequency content between 5 and 22 Hz (Figure 4a); b) with two frequency peaks at 5-22 Hz and 25-30 Hz (Figure 4b); c) with a relatively flat distribution with no dominant spectral peak (Figure 4c). The relationship between maximum amplitude and the ratio PSD_{LOW}/PSD_{HIGH} (where PSD_{LOW} corresponds to the 5-22 Hz interval and PSD_{HIGH} corresponds to the 25-30 Hz range) shows a positive trend, indicating that events with higher seismic amplitude consistently show a greater dominance of the low-frequency spectral peak over the high-frequency one (Figure 5a). A similar trend is observed plotting the maximum amplitude vs. the peak frequency in both spectral ranges (Figure 5b). First, higher-amplitude events tend to have their low-frequency peak located at lower frequencies within the 5–22 Hz range: #233 peaks at 17.1 Hz, while weaker events such as #155, #253, #256, and #265 peak near 20–21 Hz (Table 1). Second, the high-frequency peak also shifts downward in more energetic events, with #233 and #165 peaking near 25–26 Hz compared to 28–29 Hz for the weakest events. The low-frequency peak of the #213 event (15.8 Hz) is not representative, since it corresponds to the lahar which has a flat frequency distribution (Figure 4c). This tendency is confirmed by plotting the ratio of PSD_{LOW} vs PSD_{HIGH} in terms of maximum amplitude (Figure 5c).

4.2 Image analysis: morphological changes of the channel and characteristics of the lahars.

Available images were analyzed to detect temporal changes in the ravine's morphology during the 2025 season. During this rainy season, the main changes in the channel were in depth or width. An exact measurement of these changes could not be determined; however, based on a visual scale (Figure 2c), they were on the

article in press

order of <1 m. Lateral terraces showed sediment deposition only after the main event on 21 August 2025 (Figure 6a and b); for the other lahars, the main changes were restricted to the inner channel section, and were mostly erosive (Figure 6c and d). Based on the images, the maximum flow depth on 21 August 2025 was estimated at around 1.5 m; large blocks are observed rolling on the channel bed during flowage. The other events remain confined to the active channel, which is ~0.5 m deep. Based on images acquired since 2018, channel morphology has remained quite constant; major changes occurred in 2021 and 2023 due to the passage of two main lahars (Figure 6e-h). These two events overspilled the main channel with an evident enrichment in blocks and sediment content compared to the larger event detected in 2025. No seismic data are available for these events.

4.3 Rainfall data

From the daily record, 831 rainfall events were identified, accumulating 901.6 mm from June to October, which represents the area average (Carrera-Hernández, 2025) (Tables 2 and S1). For each rainfall event, the total accumulated rainfall (R), duration (D), average intensity (I_A), and maximum peak intensity (I_5) were calculated and used to identify a possible correlation between rainfall characteristics and lahar occurrence (Table 2). The ID number in Figure 7 identifies each detected rainfall event (Tables 2 and S1). The rainfall events associated with lahars correspond to the highest values of accumulated rainfall and intensity (Figures 7a and b). In particular, 9 mm of total accumulated rainfall emerges as a possible threshold distinguishing rainfall events that trigger lahars from those that do not. Above this threshold, lahar-triggering rainfall events exhibit average and peak intensities exceeding 7.9 and 21.6 mm h^{-1}, respectively. The average intensity-duration chart (Figure 7c) can also separate high-intensity rainfall episodes that triggered lahars from the vast majority of other rainfall episodes that did not cause lahars. These events fall between the thresholds proposed by Staley et al., (2013) for post-fire debris flows in Southern California and those proposed by Berti and Simoni (2005) for alpine catchments. Finally, for most of the events, the maximum peak intensity is more than twice the average intensity (Figure 7d).

article in press

5. Discussion

The 2025 rainy season dataset constitutes the first systematic record of rainfall-triggered lahars at Popocatépetl volcano based on real-time visual and seismic monitoring. Although a single season of data cannot be considered fully representative of the range of lahar activity at this volcano, it provides a valuable baseline for characterizing the seismic response of these flows and for developing objective detection criteria applicable to operational monitoring. The monitoring station was installed in late 2019; however, a reliable transmission link was not established until 2024, and the 2024 record was too intermittent to be included in the present analysis. The 2025 dataset is therefore treated as the first continuous and sufficiently complete record available for systematic lahar characterization.

5.1 Seismic signatures of lahars at Popocatépetl volcano.

The amplitude and frequency content of lahar seismic signals are known to reflect flow magnitude (depth), sediment concentration (Doyle et al., 2011, Coviello et al., 2019; Suwa et al., 2000; Walsh et al., 2020), and grain-size distribution (Coviello et al., 2018; Lai et al., 2018; Zhang et al., 2021). In particular, lahar-induced seismic signals have been reported over a frequency range of 10–100 Hz (Marcial et al., 1996), with flows of higher sediment concentration generally exhibiting greater low-frequency (<50 Hz) seismic energy, whereas more dilute flows are characterized by relatively higher-frequency (>50 Hz) energy (Cole et al., 2009; Doyle et al., 2010). At Volcán de Colima (Mexico), where the seismic sensor is located 40 m from the channel, a well-defined correlation between flow depth and seismic amplitude has been established (Martínez-Valdés et al., 2023; Márquez-Ramírez et al., 2025). In that system, amplitudes exceeding 0.3 mm/s are associated with debris flows deeper than 2 m characterized by block-rich surge fronts, with dominant PSD energy concentrated in the 10–11 Hz range. As flow depth and sediment concentration decrease, a secondary PSD peak emerges at approximately 20 Hz, indicative of hyperconcentrated flows, which eventually dominates in dilute, fluvial conditions (Pierson and Costa, 1987). These absolute thresholds are site-specific and cannot

article in press

be directly transferred to other volcanoes, given the strong dependence of seismic amplitude on sensor–channel distance and channel geometry (Arattano et al., 2015; Kean et al., 2015; Lai et al., 2018; Allstadt et al., 2019). However, the relative trends in amplitude and spectral content provide a transferable framework for interpreting lahar type and magnitude at other monitoring sites. Similar seismic characteristics have been observed in both experimental studies and natural debris flows (Yang et al., 2024).

Applying this framework to the Popocatépetl dataset, the event recorded on 21 August 2025 (#233, Table 1) stands out clearly from the others, with a maximum amplitude of 1.19 mm/s, one to two orders of magnitude higher than the remaining events (Table 1). Its PSD is dominated by energy in the 5-22 Hz band, whereas the other lahars exhibit secondary peaks at higher frequencies with PSD values two to four times lower (Figure 5a). Image analysis confirms that this event produced the deepest flow, capable of overflowing the main channel and transporting clasts several tens of centimeters in diameter, and is here interpreted as a hyperconcentrated flow (Figure 6a and b). The remaining events were confined to the active channel and appeared more muddy in the camera imagery, likely diluting to fluvial currents (Figure 6c and d). Detailed analysis of amplitude variation in the two frequency ranges (low, 5-22 Hz and high, 25-30 Hz) reveals a clear spectral trend. The relationship between maximum amplitude and the PSD_{LOW}/PSD_{HIGH} ratio shows a positive trend, indicating that events with higher seismic amplitude consistently exhibit a greater dominance of the low-frequency spectral peak over the high-frequency one (Figure 5a). Events with the PSD_{LOW}/PSD_{HIGH} ratio > 3× (PSD_{LOW} three times greater than PDS_{HIGH}), particularly #233 and #165, correspond to the largest and most energetic flows, while events with a ratio < 3x cluster toward lower amplitudes and more balanced spectral energy between both frequency bands. This pattern supports the interpretation that larger lahars, likely carrying higher sediment loads, larger clasts and with greater flow depths, generate seismic energy preferentially concentrated at lower frequencies, while smaller or more dilute flows show a more comparable contribution from both spectral bands (Huang et al., 2007; Yang et al., 2024; Márquez-Ramírez et al., 2025). A similar trend is observed

article in press

plotting the maximum amplitude vs. the peak frequency in both spectral ranges (Figure 5b).

First, higher-amplitude events tend to have both low-frequency and high-frequency spectral peaks toward lower values in both spectral ranges (5-22 Hz and 25-30 Hz). This systematic downward shift with increasing amplitude is consistent with the mechanical behavior expected of denser, deeper flows transporting larger clasts, which generate lower-frequency signals (Huang et al., 2004; Farin et al., 2019). This pattern is also consistent with observations at Volcán de Colima, where a comparable downward migration of peak frequency is observed between debris flow and hyperconcentrated flow, reinforcing our model, in which frequency content can strongly indicate sediment concentration and, consequently, grain size.

The same tendency is observable plotting PSD_{LOW} vs PDS_{HIGH} (Figure 5c), confirming that in every case the low-frequency peak carries more power than the high-frequency peak. However, the distance from the 1:1 line increases with bubble size: larger events deviate more strongly above the reference line, meaning the low-frequency peak grows disproportionately faster than the high-frequency peak as flow intensity increases. This nonlinear scaling suggests that sediment load and flow depth do not simply amplify the entire seismic spectrum uniformly instead, they preferentially energize the low-frequency component. From a monitoring perspective, this implies that the PSD ratio could serve as a proxy indicator of flow intensity, potentially useful for real-time classification of lahar severity from seismic data alone.

Finally, a comparative analysis is performed with data published for lahars at Volcán de Colima. Plotting maximum amplitude against PSD peak values in the 5-22 Hz band reveals a consistent trend: as amplitude decreases, PSD values decrease, indicating a progressive shift from higher-energy, sediment laden flows (hyperconcentrated flow) toward more dilute conditions (fluviatile current) (Figure 8a). This behavior mirrors the pattern documented at Volcán de Colima (Márquez-Ramírez et al., 2025) and for non-volcanic debris flows (Yang et al., 2024), supporting its applicability as a general flow-type classification approach. The

article in press

proximity of the sensor to the channel at Popocatépetl (~8 m) explains why the largest lahar recorded here, with a flow depth of only ~1.5 m, yields a higher maximum amplitude than much larger debris flows (>3 m depth, with meter-sized blocks) detected at Volcán de Colima 40 m from the channel (Figure 8b and c). As noted, lahar amplitude and frequency signals often depend on channel geometry and distance from the sensor (Lai et al., 2018; Huang et al., 2004; Thouret et al., 2020). Notwithstanding these absolute differences, the relative spectral and amplitude trends are consistent across both systems.

The monitoring station was intentionally positioned at the outlet of the Huiloac–Tenenpanco watershed (Figure 1), the transition point beyond which depositional processes dominate over erosion. Downstream of this location, detected flows enter a narrow, densely vegetated channel where progressive dilution is expected, as documented for the 1998 and 2001 lahars, the largest events in this ravine over the past four decades, which transitioned from debris flow to hyperconcentrated flow deposits before reaching the town of Santiago Xalitzintla at 15 km from the crater (Capra et al., 2004). Given this context and based on the seismic and image data presented here, a detection threshold of 1 mm/s is proposed for lahars detected at the HMS site. This value would allow operational monitoring systems to distinguish hyperconcentrated flows/debris flows, which retain erosive and depositional capacity along the downstream reach, from dilute, fluviatile events unlikely to cause damage. Consistent with this interpretation, none of the events recorded during the 2025 season were reported by residents at Santiago Xalitzintla, confirming that even the largest event (#233) did not produce flows hazardous enough to affect populated areas downstream. This threshold should be treated as a first approximation and refined as additional seasons of data become available.

5.2 Rainfall

The rainfall data analyzed here were collected at the monitoring station and therefore reflect conditions at a single point on the lower flank of the volcano, which may not accurately represent the rainfall driving lahar initiation in the upper catchment. This spatial mismatch is an inherent limitation of single-gauge monitoring in mountainous

article in press

terrain, as also noted at Volcán de Colima, where rainfall can be highly variable across the catchment, particularly at the onset of the rainy season (Capra et al., 2010). Notwithstanding this limitation, a clear positive relationship is observed between total accumulated rainfall and average and peak intensity across the 2025 dataset (Figure 7). Most rainfall events are characterized by low accumulation and low intensity and do not produce detectable lahar activity. Lahars were consistently associated with accumulated totals exceeding 9 mm and average intensities above 10 mm/h for most events, with peak intensities over 20 mm/h. These rainfall events can be classified as heavy/torrential rainfall (UKMO, 2007; World Meteorological Organization, 2019). The thresholds observed here are broadly consistent with rainfall–lahar relationships documented at other volcanic systems (Lavigne et al., 2000; Capra et al., 2010; Thouret et al. 2020), as well as in non-volcanic environments (Berti and Simoni, 2005; Staley et al., 2013) (Figure 7c), and offer further support to their applicability for Popocatépetl. Some detected lahars deviate from this trend, likely reflecting spatial variability in rainfall between the monitoring station and the source area. An example of this variable spatial rainfall distribution can be observed by comparing the values recorded at the monitoring station with those obtained at the Tenenpanco raingauge (R*, Table 2 and Figure 1b). Despite this uncertainty, these values can serve as preliminary triggering thresholds for this drainage system.

6. Conclusion

This study presents the first seismic characterization of rainfall-triggered lahars at Popocatépetl volcano, based on data collected during the 2025 rainy season at a real-time monitoring station on the NW flank of the volcano. The main findings and their implications can be summarized as follows. Nine lahar events were identified from continuous seismic records, with seismic amplitudes spanning two orders of magnitude. Three signal types were distinguished on the basis of PSD distributions and dominant frequency content (5–22 Hz), reflecting a spectrum of flow conditions from debris flow to dilute fluvial transport. The largest event, recorded on 21 August 2025, reached an amplitude of 1.19 mm/s and produced a flow capable of

article in press

overflowing the main channel; the remaining events were confined within the active channel and exhibited more dilute, fluvial characteristics. A positive correlation between seismic amplitude and PSD peak frequency at 5–22 Hz provides a basis for classifying lahar type and relative magnitude in real time, with main peak frequencies shifting to higher values as lahar magnitude (i.e., sediment content) decreases. These observations are consistent with patterns documented at Volcán de Colima and non-volcanic debris flow systems. Rainfall thresholds of >9 mm accumulated and >20 mm/hr peak intensity (5-minute windows) are proposed as necessary conditions for lahar triggering at the Huiloac–Tenepanco drainage. At this site, a seismic detection threshold of 1 mm/s is proposed to operationally distinguish hyperconcentrated flows from lower-magnitude fluvial events unlikely to pose a hazard to downstream communities. The Huiloac ravine remains the most active drainage for rain-triggered lahars at Popocatépetl, and the monitoring infrastructure established there constitutes a foundational element of an early warning system for one of the most densely populated volcanic areas in the world.

Declaration of competing interest

The authors declare that they have no known competing financial interests or personal relationships that could have appeared to influence the work reported in this paper.

Author Contributions

VH Márquez-Ramírez: Writing review & editing, Software, Methodology, Investigation, Data curation, Conceptualization, Formal analysis, Writing original draft. **Lucia Capra**: Writing review & editing, Software, Methodology, Visualization, Project administration, Investigation, Funding acquisition, Formal analysis, Conceptualization, Writing original draft. **P.C. Ávila, P. Alonso Rivera, G. Castelán-Pescina**: Writing review & editing, Visualization, Software, Data curation.

article in press

Declaration of generative AI and AI-assisted technologies in the writing process

Grammarly tool was used in order to improve grammar and spelling. After using this tool/service, the authors reviewed and edited the content as needed and take full responsibility for the content of the publication.

Acknowledgments

CONAHCyT project PDCPN-2015-360 to LC (for the instrumentation of the monitoring site), PAPIIT IN109825 and L'Oréal-UNESCO-AMC Prize to LC. Authors express their acknowledgment to Centro Nacional de Prevención de Desastres (CENAPRED) for logistic support. We are also grateful to two anonymous reviewers for their constructive and insightful comments.

Data availability

We processed seismic signals using the ObsPy v. 1.5 (Krischer et al., 2015) and SciPy v. 1.16.3 (Virtanen et al., 2020) Python libraries. Figures were produced using Matplotlib v. 3.10.8 (Hunter, 2007). Raw data are available from the corresponding author. The complete technical specifications and instrument response for the RS-4D can be consulted at https://manual.raspberryshake.org/specifications.html

References

Allstadt, K.E., Farin, M., Lockhart, A.B., McBride, S.K., Kean, J.W., Iverson, R.M., Logan, M., Smith, J.B., Tsai, V.C., George, D., (2019). Overcoming barriers to progress in seismic monitoring and characterization of debris flows and lahars. In: Debris-Flow Hazards Mitigation: Mechanics, Monitoring, Modeling, and Assessment — Proceedings of the 7th International Conference on Debris-Flow Hazards Mitigation, Golden, Colorado, 10–13 June 2019. Colorado School of Mines. http://dx.doi.org/10.25676/11124/173234

Anthony, R.E., Ringler, A.T., Wilson, D.C., Wolin, E., (2019). Do low-cost seismographs perform well enough for your network? An overview of laboratory tests

article in press

and field observations of the OSOP Raspberry Shake 4D. Seismological Research Letters 90 (1), 219-228. https://doi.org/10.1785/0220180251

Arámbula-Mendoza, R., Valdés-González, C., Varley, N., Reyes-Pimentel, T.A., Juárez-García, B., (2016). Tremor and its duration–amplitude distribution at Popocatépetl volcano, Mexico. *Geophysical Research Letters* 43, 8994–9001. https://doi.org/10.1002/2016GL070227

Arattano, M., & Turconi, L., (2015). Detecting torrential processes from a distance with a seismic monitoring network. Natural Hazards, 78, 2129–2144. https://doi.org/10.1007/s11069-015-1819-2

Barclay, J., Alexander, J., Sušnik, J., (2007). Rainfall-induced lahars in the Belham Valley, Montserrat, West Indies. *J Geol Soc London* **164**, 815–827. https://doi.org/10.1144/0016-76492006-078

Bejar, G., Waite, G. P., Escobar-Wolf, R., Chatterjee, S., Bosa, A., Roca, A., Johnson, J.B., Mock, J., Pineda, A., (2026). Seismic Characterization of Lahars on Volcán de Fuego Toward the Development of a Machine Learning-Based Detection Algorithm. J. Geophys. Res.: Solid Earth 131. https://doi.org/10.1029/2025JB032019.

Berti, M., Simoni, A., (2005). Experimental evidences and numerical modelling of debris flow initiated by channel runoff. *Landslides* **2**, 171–182. DOI: 10.1007/s10346-005-0062-4.

Bosa, A., Johnson, J. B., De Angelis, S., Lyons, J., Roca, A., Anderson, J. and Pineda, A. (2021). Tracking secondary lahar flow paths and characterizing pulses and surges using infrasound array networks at Volcán de Fuego, Guatemala. *Volcanica* **4**, 239–256. https://doi.org/10.30909/vol.04.02.239256

Bosa, A.R., Bejar, G., Waite, G.P., Mock, J.C., Pineda, A., Anderson, J.F., (2024). Dynamics of rain-triggered lahars and destructive power inferred from seismo-acoustic arrays and time-lapse camera correlation at Volcán de Fuego, Guatemala. *Nat. Hazards* 1–42 doi:10.1007/s11069-024-06926-1.

article in press

Capra, L., Poblete, M.A., Alvarado, R., (2004). The 1997 and 2001 lahars of Popocatépetl volcano (Central Mexico): textural and sedimentological constraints on their origin and hazards. *J. Volcanol. Geotherm. Res.* 131, 351–369. https://doi.org/10.1016/S0377-0273(03)00386-8

Capra, L., Borselli, L., Varley, N., Gavilanes-Ruiz, J.C., Norini, G., Sarocchi, D., Caballero, L., Cortés, A., (2010). Rainfall-triggered lahars at Volcán de Colima, Mexico: surface hydro-repellency as initiation process. *J. Volcanol. Geotherm. Res.* 189, 105–117. https://doi.org/10.1016/j.jvolgeores.2009.10.014

Carrera-Hernández, J.J., (2025). Mexico's High Resolution Climate Database (MexHiResClimDB): a new daily high-resolution gridded climate dataset for Mexico covering 1951–2020, Earth Syst. Sci. Data, 17, 6911–6941, https://doi.org/10.5194/essd-17-6911-2025

Carrivick, J. L., Manville, V., Cronin, S. J., (2009). A fluid dynamics approach to modelling the 18th March 2007 lahar at Mt. Ruapehu, New Zealand. Bulletin of Volcanology, 71, 153–169. https://doi.org/10.1007/s00445-008-0213-2

Cole, S. E., Cronin, S. J., Sherburn, S., & Manville, V. (2009). Seismic signals of snow-slurry lahars in motion: 25 September 2007, Mt Ruapehu, New Zealand. *Geophysical Research Letters*, 36(9). https://doi.org/10.1029/2009gl038030

Coviello, V., Capra, L., Vázquez, R., Márquez-Ramírez, V.H., (2018). Seismic characterization of hyperconcentrated flows in a volcanic environment. *Earth Surf. Process. Landforms* 43, 2219–2231. https://doi.org/10.1002/esp.4387

Coviello, V., Arattano, M., Comiti, F., Macconi, P., Marchi, L., (2019). Seismic characterization of debris flows: insights into energy radiation and implications for warning. J. Geophys. Res. Earth Surf. 124, 1440–1463. https://doi.org/10.1029/2018JF004683

Coviello, V., Capra, L., Norini, G., Dávila, N., Ferrés, D., Márquez-Ramírez, V.H., Pico, E., (2021). Earthquake-induced debris flows at Popocatépetl Volcano, Mexico. *Earth Surf. Dyn.* 9, 393–412. https://doi.org/10.5194/esurf-9-393-2021

article in press

Doyle, E.E., Cronin, S.J., Cole, S.E., Thouret, J.-C., (2010). The coalescence and organization of lahars at Semeru volcano, Indonesia. Bull. Volcanol. 72, 961–970. https://doi.org/10.1007/s00445-010-0381-8

Doyle, E.E., Cronin, S.J., Thouret, J.-C., (2011). Defining conditions for bulking and debulking in lahars. *Geol. Soc. Am. Bull.* 123, 1234–1246. https://doi.org/10.1130/B30227.1

Farin, M., Tsai, V.C., Lamb, M.P., Allstadt, K.E., (2019). A physical model of the high-frequency seismic signal generated by debris flows. Earth Surface Processes and Landforms 44 (13), 2529-2543. https://doi.org/10.1002/esp.4677

Gheri, D., De Angelis, S., Pineda, A., Woodhouse, M., Phillips, J., (2026). A high-resolution seismo-acoustic and video dataset of a lahar at Volcán de Fuego, Guatemala. *Sci Data*. https://doi.org/10.1038/s41597-026-08146-7

González, A.E., 2000. Estudios de detalle estratigráfico y sedimentológico del Lahar de San Nicolás en el flanco noreste del volcán Popocatépetl. B.Sc. Thesis, Universidad Nacional Autónoma de México, Mexico, 109 pp.

Huang, C.-J., Shieh, C.-L., Yin, H.-Y., (2004). Laboratory study of the underground sound generated by debris flows. *J. Geophys. Res.* 109. https://doi.org/10.1029/2003JF000048

Huang, C. J., Yin, H. Y., Chen, C. Y., Yeh, C. H., Wang, C. L. (2007). Ground vibrations produced by rock motions and debris flows. *J. Geophys. Res* 112. https://doi.org/10.1029/2005jf000437

Huggel, C., Ceballos, J. L., PulgarÍn, B., Ramírez, J., Thouret, J.C. (2007). Review and reassessment of hazards owing to volcano–glacier interactions in Colombia. Annals of Glaciology. 45, 128–136. https://doi.org/10.3189/172756407782282408

Hungr, O., Leroueil, S., Picarelli, L., (2014). The Varnes classification of landslide types, an update. *Landslides* 11, 167–194. https://doi.org/10.1007/s10346-013-0436-y

article in press

Hunter, J.D., (2007). Matplotlib: a 2D graphics environment. Comput. Sci. Eng. 9 (3), 90–95. https://doi.org/10.1109/MCSE.2007.55

Kean, J.W., Coe, J.A., Coviello, V., Smith, J.B., McCoy, S.W., Arattano, M., (2015). Estimating rates of debris-flow entrainment from ground vibrations. Geophys. Res. Lett., 42, 6365–6372. https://doi.org/10.1002/2015GL064811

Krischer, L., Megies, T., Barsch, R., Beyreuther, M., Lecocq, T., Caudron, C., Wassermann, J., (2015). ObsPy: a bridge for seismology into the scientific python ecosystem. Comput. Sci. Discov. 8 (1), 014003. https://doi.org/doi:10.1088/1749-4699/8/1/014003

Lai, V.H., Tsai, V.C., Lamb, M.P., Ulizio, T.P., Beer, A.R., (2018). The seismic signature of debris flows: flow mechanics and early warning at Montecito, California. *Geophys. Res. Lett.* 45, 5528–5535. https://doi.org/10.1029/2018GL077683

Lavigne, F., Thouret, J.-C., Voight, B., Young, K., LaHausen, R., (2000). Instrumental lahar monitoring at Merapi Volcano, Central Java, Indonesia. *J Volcanol Geoth Res* 100, 457–478. https://doi.org/10.1016/S0377-0273(00)00151-7

Lavigne, F., Thouret, J.-C., (2002). Sediment transportation and deposition by rain-triggered lahars at Merapi Volcano, Central Java, Indonesia. *Geomorphology* 49, 45–69. https://doi.org/10.1016/S0169-555X(02)00160-5

Macías, J.L., Capra, L., Scott, K.M., Espíndola, J.M., García-Palomo, A., Costa, J.E., (2004). The 26 May 1982 breakout flows derived from failure of a volcanic dam at El Chichón, Chiapas. *GSA Bull.* 116, 233-246. https://doi.org/10.1130/B25318.1

Macías, J.L., Arce, J.L., García-Tenorio, F., Sosa-Ceballos, G., Gardner, J.E., (2020). Source and behavior of pyroclastic density currents generated by Vulcanian-style explosions of Popocatépetl volcano (Mexico) on 22 January 2001. *J. Volcanol. Geotherm. Res.* 406, https://doi.org/10.1016/j.jvolgeores.2020.107071.

Marcial, S., Melosantos, A. A., Hadley, K. C., La Husen, R., Marso, J. N. (1996). Instrumental lahar monitoring at Mount Pinatubo. In C. G. Newhall & A. S.

article in press

Punongbayan (Eds.), Fire and mud: Eruptions and lahars of Mount Pinatubo, Philippines. Hong Kong: Philippine Institute of volcanology and seismology.

Márquez-Ramírez, V.H., Capra, L., Martínez-Valdés, J.I., Barroso-Fernández, R., Arámbula-Mendoza, R., González Amezcua, M., García Flores, R., (2025). Seismic classification of rainfall-induced lahars at Volcán de Colima, México: frequency content as an indicator of sediment concentration. *J. South Am. Earth Sci.* 167, 105768. https://doi.org/10.1016/j.jsames.2025.105768

Martínez-Valdés, J.I., Márquez-Ramírez, V.H., Coviello, V., Capra, L., (2023). Hurricane-induced lahars at Volcán de Colima (México): seismic characterization and numerical modeling. *Rev. Mex. Cienc. Geol.* 40, 59–70. https://doi.org/10.22201/cgeo.20072902e.2023.1.1709

Muñoz-Salinas, E., Castillo-Rodríguez, M., Manea, V., Manea, M., Palacios, D., (2009). Lahar flow simulations using LAHARZ program: application for the Popocatépetl volcano, Mexico. *J. Volcanol. Geotherm. Res.* 182, 13–22. https://doi.org/10.1016/j.jvolgeores.2009.01.030

Pierson, T. C. & Scott, K. M. (1985). Downstream Dilution of a Lahar: Transition From Debris Flow to Hyperconcentrated Streamflow. *Water Resour Res* **21**, 1511–1524. https://doi.org/10.1029/WR021i010p01511

Pierson, T.C., Costa, J.E., (1987). A rheologic classification of subaerial sediment-water flows. *Geol. Soc. Am. Rev. Eng. Geol.* 7, 1–12. https://doi.org/10.1130/REG7-p1

Scott, K.M., Vallance, J.W., Pringle, P.T., (1995). Sedimentology, behavior, and hazards of debris flows at Mount Rainier, Washington. *U.S. Geol. Surv. Prof. Pap.* 1547, 56 pp. https://doi.org/10.3133/pp1547

Siebe, C., Abrams, M., Macías, J.L., Obenholzner, J., (1996). Repeated volcanic disasters in Prehispanic time at Popocatépetl, central Mexico: past key to the future? *Geology* 24, 399–402. https://doi.org/10.1130/0091-7613(1996)024<0399:RVDIPT>2.3.CO;2

article in press

Siebe, C., Schaaf, P., Urrutia-Fucugauchi, J., (1999). Mammoth bones embedded in a late Pleistocene lahar from Popocatépetl volcano, near Tocuila, central México. *GSA Bull.* **111**, 1550–1562. https://doi.org/10.1130/0016-7606(1999)111<1550:MBEIAL>2.3.CO;2

Siebe, C. Salinas, S., Arana-Salinas, L., Macías, J.L., Gardner, J., Bonasia, R., (2017). The ~23,500y 14C BP White Pumice Plinian eruption and associated debris avalanche and Tochimilco lava flow of Popocatépetl volcano, México. *J. Volcanol. Geotherm. Res.* **333**, 66–95. https://doi.org/10.1016/j.jvolgeores.2017.01.011

Siebe, C., Ramírez-Uribe, I., Macías, J. L. & Böhnel, H., (2024). Radiocarbon dating, magnitude, and catastrophic impact of Popocatépetl's Terminal Preclassic "Lorenzo pumice" Plinian eruption and paleomagnetic age constraints on the Nealtican lava flow field (central Mexico). *J. Volcanol. Geotherm. Res..* **445**, 107974 https://doi.org/10.1016/j.jvolgeores.2023.107974

Smith, G. A. & Lowe, D. R., (1991). Lahars: volcano-hydrologic events and depostion in the debris flow-hyperconcentrated flow continuum. in Sedimentation in volcanic settings, Fisher, R. V. & Smith, G. A.(eds). *SFPM Special Publication* No. 45, pp. 59-70. ISBN 0-918985-89-7

Sosa-Ceballos, G., Gardner, J.E., Siebe, C., Macías, J.L., (2012). A caldera-forming eruption ~14,100 14C yr BP at Popocatépetl volcano, Mexico: insights from eruption dynamics and magma mixing. J. Volcanol. Geotherm. Res. 213–214, 27–40. https://doi.org/10.1016/j.jvolgeores.2011.11.001

Staley, D. M., Kean, J. W., Cannon, S. H., Schmidt, K. M. & Laber, J. L., (2013). Objective definition of rainfall intensity–duration thresholds for the initiation of post-fire debris flows in southern California. Landslides 10, 547–562. DOI 10.1007/s10346-012-0341-9.

Suwa, H., Yamakoshi, T., Sato, K., (2000). Relationship between debris-flow discharge and ground vibration, in Debris-Flow Hazards Mitigation: Mechanics, Prediction, and Assessment: Proceedings of the Second International Conference, pp. 311–318, A. A. Balkema, Brookfield, Vt.

article in press

Tary, J. B., Herrera, R. H., Han, J. y van der Baan, M. (2014). Spectral estimation — what is new? What is next?. Reviews of Geophysics, 52, 723–749. http://doi.org/10.1002/2014RG000461

Thouret, J.-C., Antoine, S., Magill, C., Ollier, C., (2020). Lahars and debris flows: characteristics and impacts. *Earth-Sci. Rev.* 201, 103003. https://doi.org/10.1016/j.earscirev.2019.103003

UKMO (United Kingdom Meteorological Office), (2007). Fact sheet no. 3: Water in the atmosphere, Tech. rep., United Kingdom Meteorological Office. Available at https://www.metoffice.gov.uk/api/assets/file/factsheet_3-water-in-the-atmosphere_2023pdf?prefix=assets

Vázquez, R., Suriñach, E., Capra, L., Arámbula-Mendoza, R., Reyes-Dávila, G., (2016). Seismic characterization of lahars at Volcán de Colima, Mexico. Bulletin of Volcanology, 78, 8. https://doi.org/10.1007/s00445-016-1004-9

Virtanen, P., Gommers, R., Oliphant, T.E., Haberland, M., Reddy, T., Cournapeau, D., Burovski, E., Peterson, P., Weckesser, W., Bright, J., et al., (2020). Scipy 1.0: fundamental algorithms for scientific computing in python. Nat. Methods 17 (3), 261–272. https://doi.org/10.1038/s41592-019-0686-2

Walsh, B., Coviello, V., Capra, L., Procter, J., Márquez-Ramírez, V.H., (2020). Insights into the internal dynamics of natural lahars from analysis of 3-component broadband seismic signals at Volcán de Colima, Mexico. Front. Earth Sci. 8, 542116. https://doi.org/10.3389/feart.2020.542116

Welch, P.D., (1967). The use of fast Fourier transform for the estimation of power spectra: a method based on time averaging over short, modified periodograms. *IEEE Trans. Audio Electroacoust.* 15, 70–73. https://doi.org/10.1109/TAU.1967.1161901

World Meteorological Organization, (2019). WMO Statement on the state of the global climate in 2018. WMO-No. 1233, Geneva, 978-92-63-11233-0 https://library.wmo.int/idurl/4/56141

article in press

652 Yang, Y., Chen, G., Li, Y., Meng, X., Chong, Y., Bian, S., Jin, J., Shi, W., Wu,
653 J., Yue, D., (2024). Characterization of stream, hyperconcentrated and debris flows
654 from seismic signals: insights into sediment transport mechanisms and flow
655 dynamics. *J. Geophys. Res. Earth Surf.* 129, e2023JF007527.
656 https://doi.org/10.1029/2023JF007527

657 Zaragoza, G., Caballero-García, L., Capra, L., Nieto-Torres, A., (2020).
658 Secondary lahars at Popocatépetl volcano: the Nexpayantla lahar of February 4th,
659 2010. *Rev. Mex. Cienc. Geol.* 37, 121–134.
660 https://doi.org/10.22201/cgeo.20072902e.2020.2.1565

661 Zhang, Z., Walter, F., McArdell, B. W., Wenner, M., Chmiel, M., de Haas, T.,
662 He, S., (2021). Insights from the particle impact model into the high-frequency
663 seismic signature of debris flows. Geophysical Research Letters, 48(1)
664 https://doi.org/10.1029/2020GL088994

665 Zobin, V., (2017). Introduction to Volcanic Seismology, 3rd Edition, Elsevier,
666 **ISBN:** 978-0-444-63631-7 https://doi.org/10.1016/C2015-0-00304-5
667

article in press

Figure

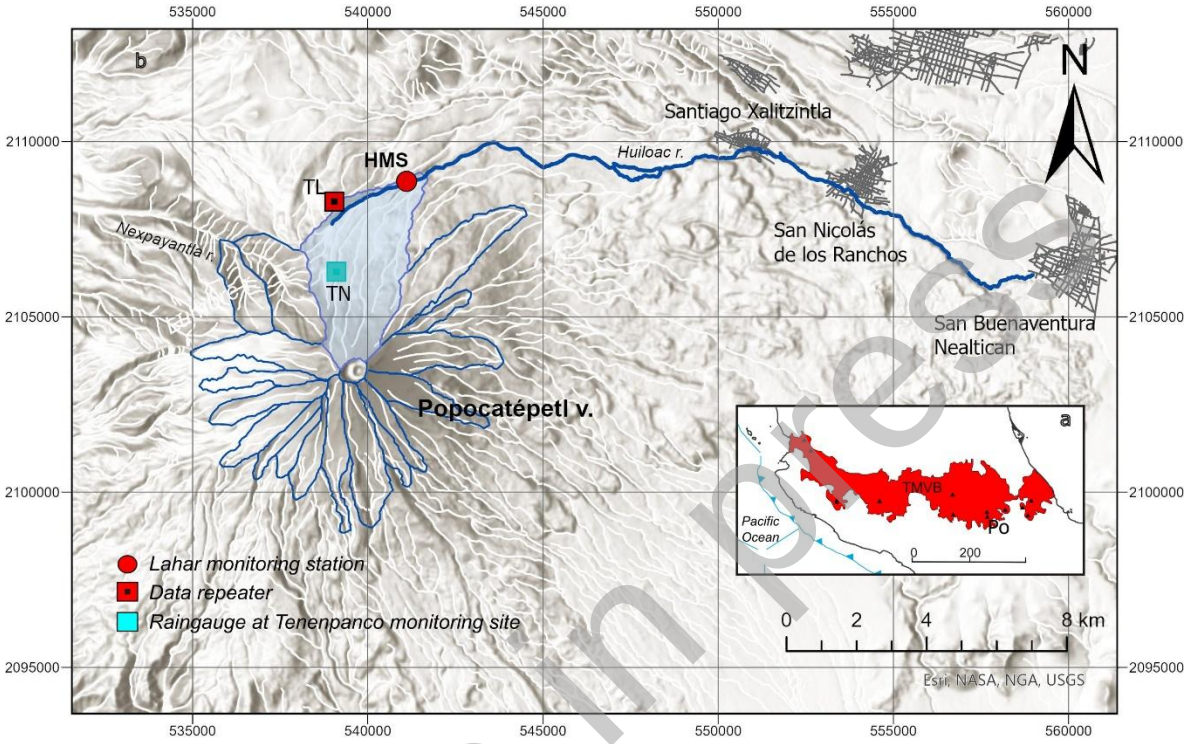


Figure 1. a) Sketch map of the location of Popocatépetl volcano along the Trans-Mexican Volcanic Belt (TMVB). Black triangles indicate the main active volcanoes in Mexico. b) Topographic map of Popocatépetl volcano and the location of the lahar monitoring station along the Huiloac River (HMS), positioned at the outlet of the main watershed that drains from the northern slope of the volcano. The blue line depicts the main trajectories of lahars that in the past affected inhabited areas. TN: Tenenpanco raingauge located along the Tenenpanco gorge; TL: Tlamacas high.

article in press

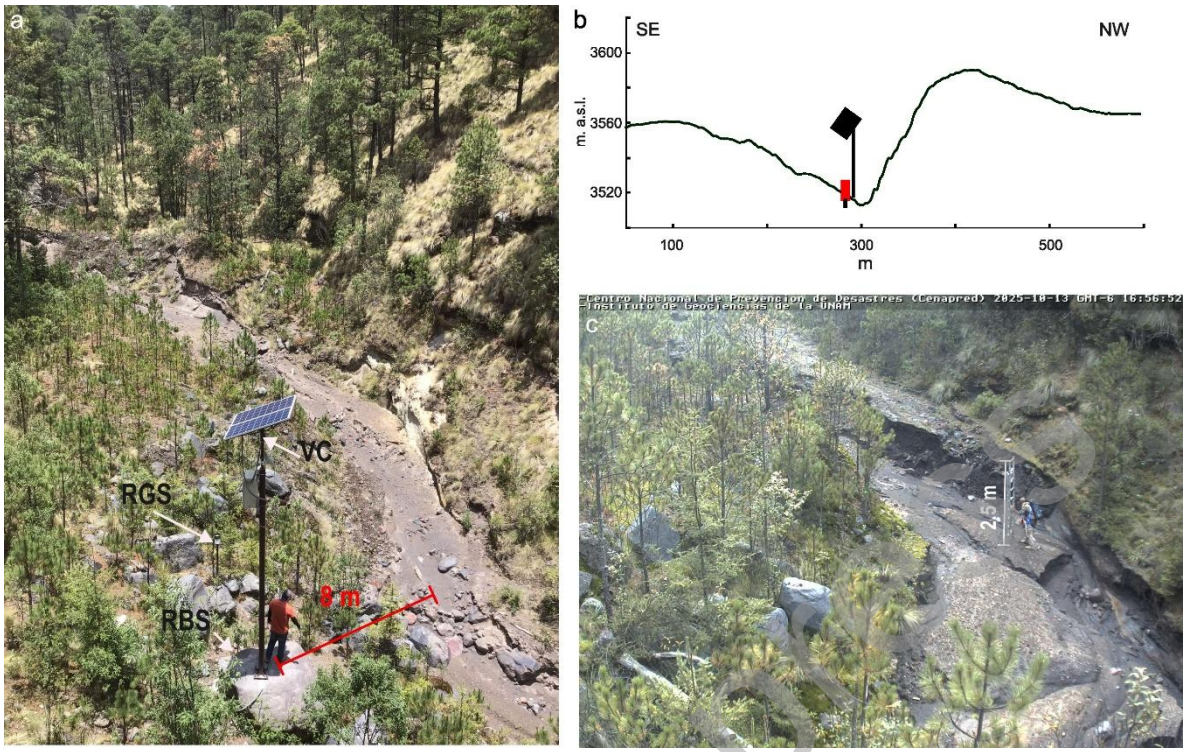


Figure 2. a) View of the monitoring station, located approximately 8 m from the main channel. VC: video camera; RGS: rain station; RBS: Raspberry Shake sensor. b) Topographic profile at the monitoring site. c) Pictures taken from the videocamera at the monitoring site with a scale reference.

article in press

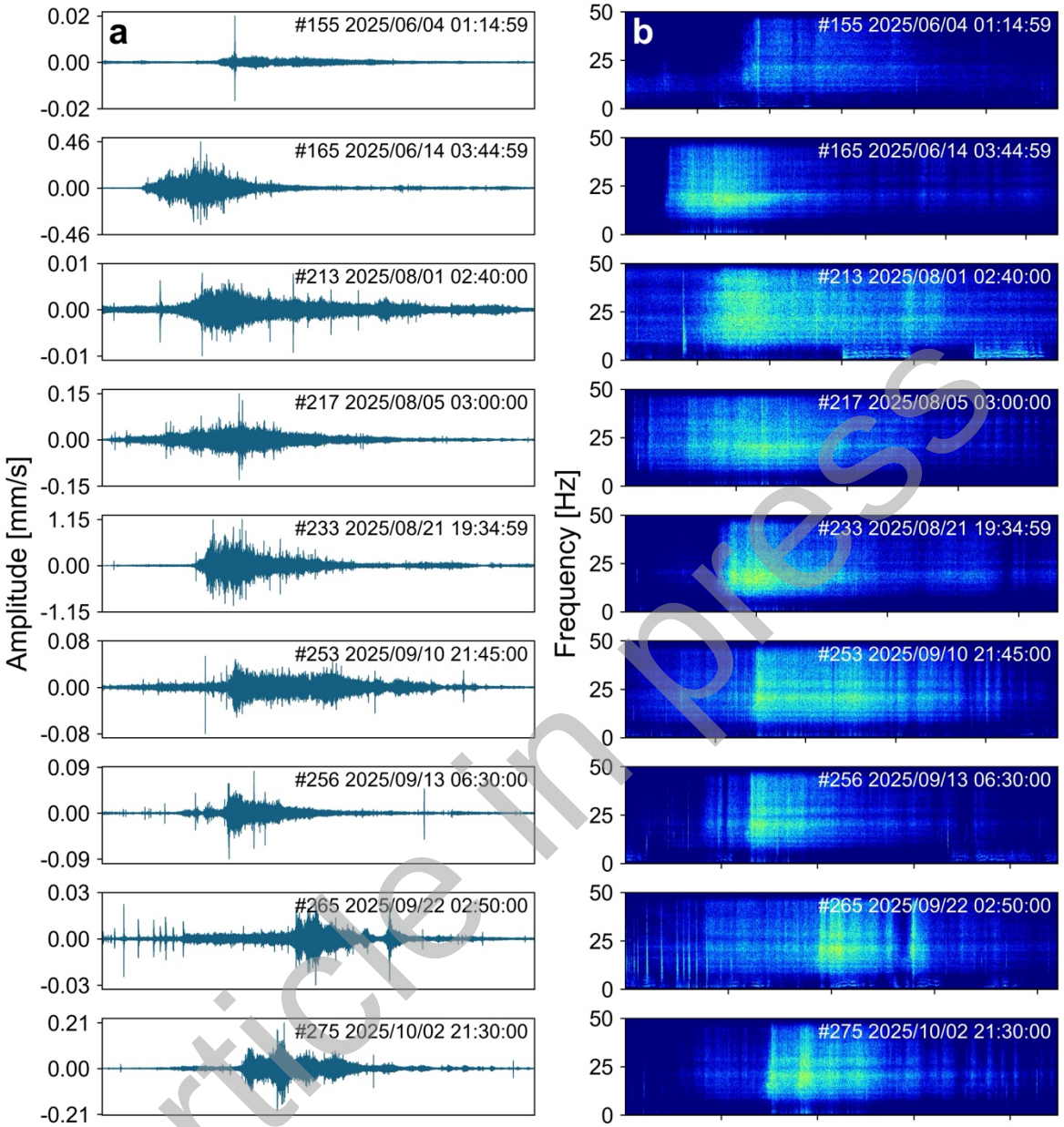
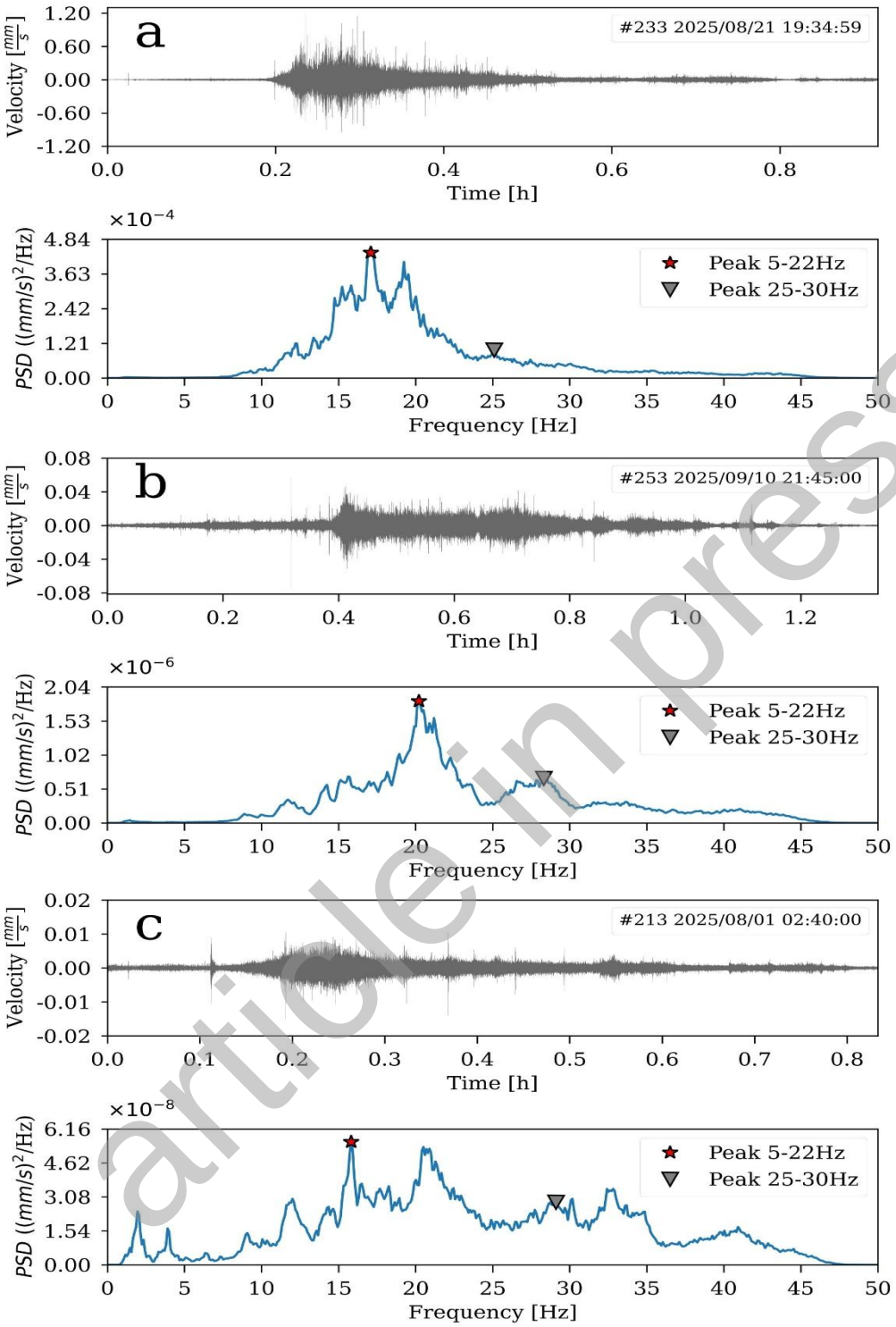


Figure 3. a) Vertical seismic signals and b) spectrograms of the nine events detected during the 2025 season. The spectrograms were calculated with 10 second windows and 50% overlap, with the same amplitude scale. The numbers of the events refer to Table 1.

article in press

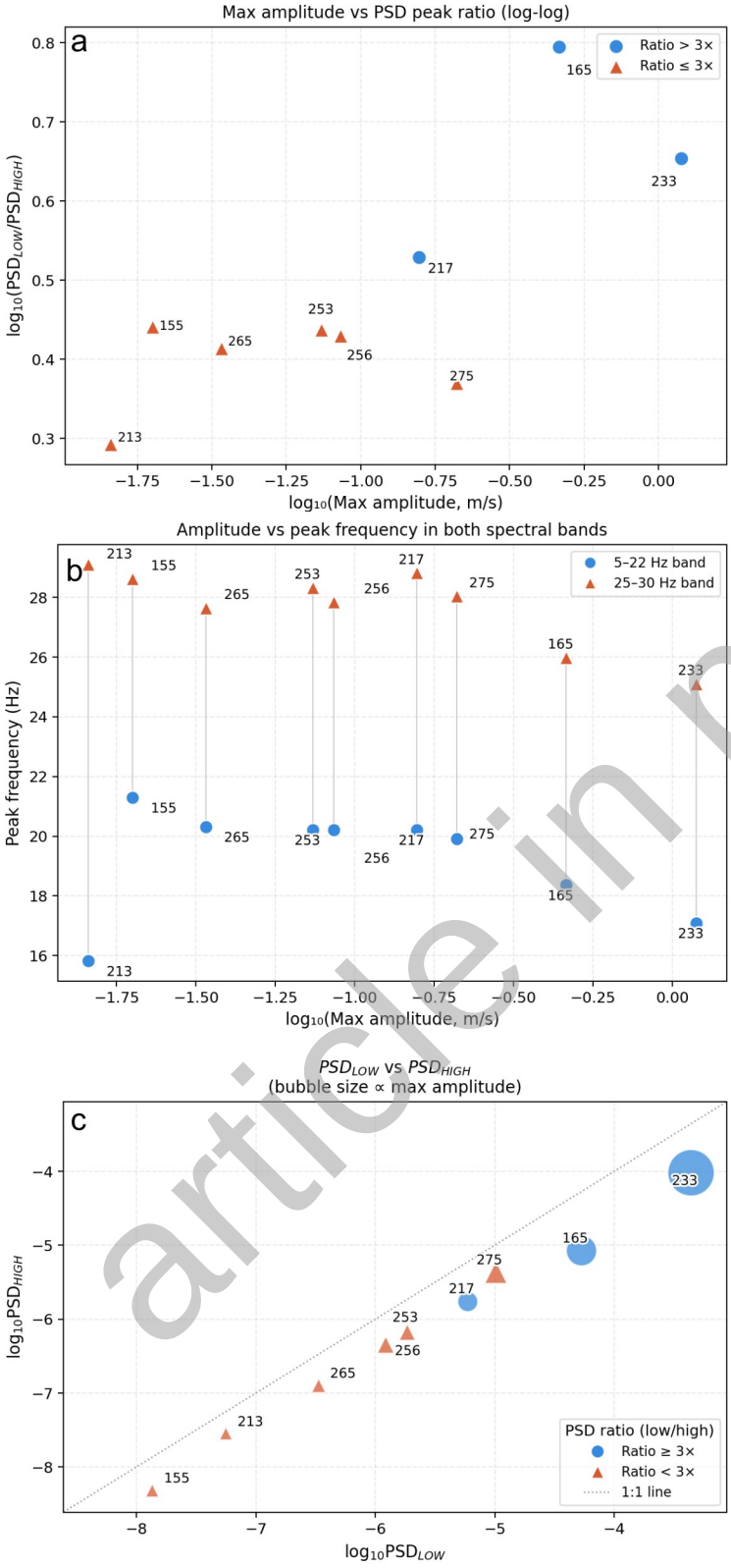


712

713 **Figure 4**. Amplitude and power spectral density (PSD) for selected events (Table 1)
714 and for each flow category. Stars and triangles refer to the maximum peak in the 5-
715 22Hz and 25-30Hz ranges, respectively.

716

article in press



article in press

Figure 5 a) Relationship between the maximum seismic amplitude of each lahar event and the ratio between the PSD value at the low-frequency peak (5–22 Hz) and

720 the PSD value at the high-frequency peak (25–30 Hz), both axes in logarithmic scale.
721 b) Difference between the high-frequency peak and the low-frequency peak against
722 event amplitude. c) Plot of the PSD at low and high frequency ranges. The dotted
723 line represents the 1:1 tendency line. Numbers identify lahars as indicated in Table
724 1.

725

726

727

728

article in press


a
14:12:06
2.5 m
21/08/2025
b
14:27:47
21/08/2025
c
10/09/2025
d
02/10/2025
e
23:00:21
20/06/2021
CENAPRED
f
23:06:21
20/06/2021
CENAPRED
g
23:08:00
08/10/2023
h
23:09:00
08/10/2023

729

Figure 6. Pictures of some selected lahars detected during the 2025 season. a) and b) refer to the largest event captured on 21 August. Note the large blocks rolling along the channel. The black dotted line refers to the mud trace left at the maximum flow depth. The other captured events remain channeled (c and d). For comparison, two of the main lahars detected since 2018 are included (e-h), but no seismic signal is available for them.

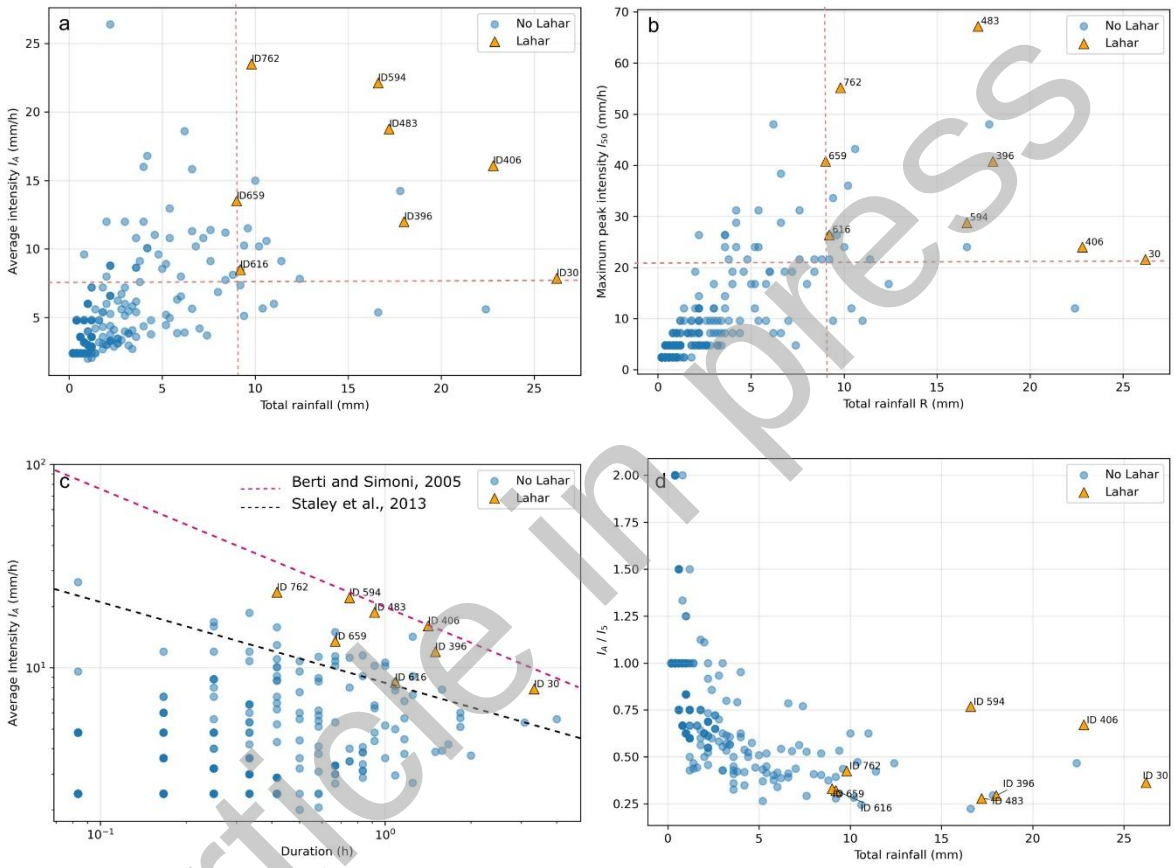


Figure 7. Total accumulated rainfall versus (a) average and (b) maximum peak rainfall intensity for the events detected at the monitoring station. Dotted lines indicate the thresholds for total accumulated rainfall and rainfall intensity above which lahars are detected. (c) Duration versus average rainfall intensity for lahar-triggering and non-triggering rainfall events, compared with existing rainfall thresholds for non-volcanic environments. (d) Relationship between rainfall duration and the ratio of average rainfall intensity to 5-min rainfall intensity. The ID-number refer to the rainfall events (Table 2).

.

article in press

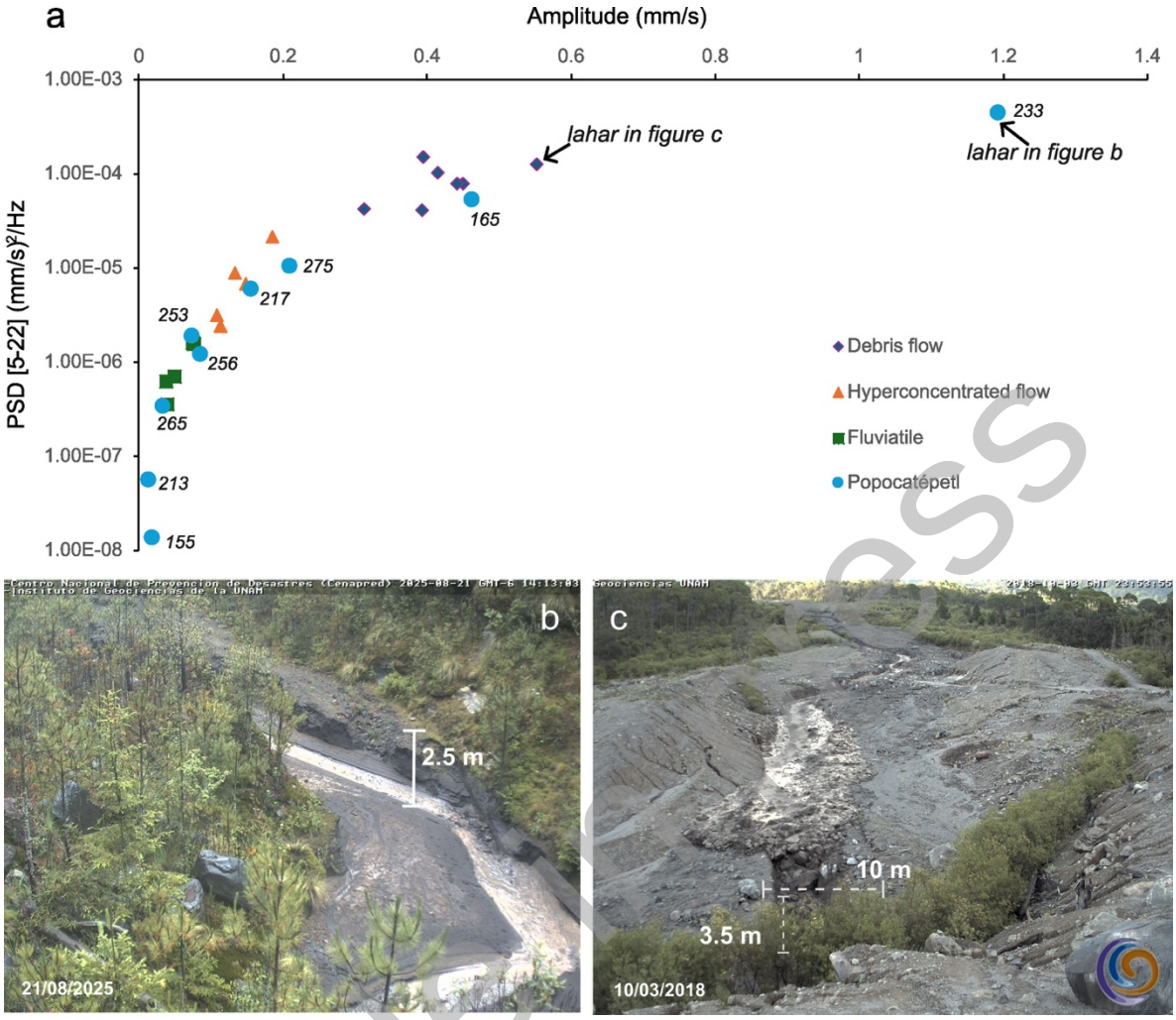


Figure 8. Amplitude vs. PSD content at 5-22 Hz frequency range of lahars at Popocatépetl and Colima volcanoes. Note that the event with the maximum amplitude corresponds to the largest lahar detected at Popocatépetl (b), and is considerably smaller in magnitude than the largest event detected at Volcán de Colima during the 2018 rainy season (c).

article in press

Table 1: Seismic parameters of recorded events

Day	Date	Max Ampl	Max_F [15-22]	Max_PSD [5-22]	Max_F [25-30]	Max_PSD [25-30]
	DD/MM/YY	mm/sec	Hz	$(mm/s)^2/Hz$	Hz	$(mm/s)^2/Hz$
155	04/06/2025	2.00E-02	21.29	1.35E-08	28.61	4.89E-09
165	14/06/2025	4.63E-01	18.36	5.28E-05	25.98	8.47E-06
213	01/08/2025	1.45E-02	15.82	5.57E-08	29.10	2.84E-08
217	05/08/2025	1.57E-01	20.21	5.92E-06	28.81	1.75E-06
233	21/08/2025	1.19E+00	17.09	4.37E-04	25.10	9.69E-05
253	10/09/2025	7.38E-02	20.21	1.83E-06	28.32	6.68E-07
256	13/09/2025	8.58E-02	20.21	1.21E-06	27.83	4.50E-07
265	22/09/2025	3.40E-02	20.31	3.32E-07	27.64	1.28E-07
275	2/10/2025	2.10E-01	19.92	1.01E-05	28.03	4.31E-06

Table 2. Rainfall characteristics for the detected lahars.

	Huiloac Monitoring Station (HMS)					TN
Day	**ID**	**R**	**D**	**I_A**	**I_5**	**R***
DD/MM/YY	record	(mm)	(min)	(mm/h)	(mm/h)	(mm)
04/06/2025	n.d.	n.d.	n.d.	n.d.	n.d.	28.42
14/06/2025	30	26.2	200	7.9	21.6	23.11
01/08/2025	396	18.0	90	12.0	40.8	n.d.
05/08/2025	406	22.8	85	16.1	24.0	2.00
21/08/2025	483	17.2	55	18.8	67.2	35.13
10/09/2025	594	16.6	45	22.1	28.8	12.9
13/09/2025	616	9.2	65	8.5	26.4	0.08
22/09/2025	659	9.0	40	13.5	40.8	n.d.
02/10/2025	762	9.8	25	23.5	55.2	4.62

ID records correspond to Table S1. R, total accumulated rainfall; D, duration; I_A: average intensity; I_5, maximum peak intensity calculated in a time window of 5 min. R* refers to the total accumulated rainfall at Tenenpanco station (TN). n.d., data not available.

article in press